Supplementary Information for: Two cations, two mechanisms: interactions of sodium and calcium with zwitterionic lipid membranes

Matti Javanainen[1,2,‡], Adéla Melcrová[3,‡], Aniket Magarkar[4,5], Piotr Jurkiewicz[3,*], Martin Hof[3], Pavel Jungwirth[4,1,*], and Hector Martinez-Seara[4,1,*]

[1] *Laboratory of Physics, Tampere University of Technology, P.O. Box 692, FI-33101 Tampere, Finland.*
[2] *Department of Physics, University of Helsinki, P.O.Box 64, FI-00014 University of Helsinki, Finland.*
[3] *J. Heyrovský Institute of Physical Chemistry, Czech Academy of Sciences, Dolejskova 3, 182 23 Prague 8, Czech Republic.*
[4] *Institute of Organic Chemistry and Biochemistry, Czech Academy of Sciences, Flemingovo nam. 2, 166 10 Prague 6, Czech Republic.*
[5] *Faculty of Pharmacy, University of Helsinki, Viikinkaari 5E, FI-00014 University of Helsinki, Finland.*
[‡] *These authors contributed equally to this work.*
[*] *E-mail: hseara@gmail.com, pavel.jungwirth@uochb.cas.cz, piotr.jurkiewicz@jh-inst.cas.cz*

Contents

S1 Computational Methods

S1.1 Simulated Single Phase Systems

The list of all studied systems is given in Table S1. Set 1 was simulated without ions and used as a reference for the effects of cholesterol alone. The Slipids [1–3] and Charmm36 [4, 5] lipid models were employed in sets **1A** and **1B**, respectively. Set 2 was employed to study the effect of cholesterol on sodium adsorption. In sets **2A** and **2B**, the Slipids force field was used with the ion parameters by Smith and Dang [6] (SD). Two different concentrations of NaCl, namely 130 mM (set **2A**) and 1 M (set **2B**) were employed. Additionally, sets **2C** and **2D** were employed to study whether the ion model [7] (MK, set **2C**) or the lipid model (Slipids vs. Charmm36 [4, 5], **2D**) affect the effect of cholesterol on sodium binding. The sodium model in Charmm36 is that derived by Noskov and Roux [8] (NR).

The binding of calcium into POPC bilayers with varying amount of cholesterol was studied in set 3 with both Slipids and Charmm36 lipid force fields. The recently published calcium and chloride ion parameters with scaled charges (MK) [7] (sets **3A** and **3B**) were employed. Additionally, these simulations were repeated with the standard ion models supplied with the Slipids and Charmm36 force fields (sets **3C** and **3D**). These default calcium parameters are the default ones supplied with Amber (AM), and the ones derived by Marchand and Roux [9] (MR).

The effect of temperature on binding of both sodium and calcium into a cholesterol-free POPC bilayers was studied using the Slipids force field in set **4**. The ion models by Smith and Dang [6] (SD) and Kohagen et al. [7] (MK) were employed for sodium and calcium, respectively.

The binding of sodium and calcium into L_d phase cholesterol-free DOPC bilayers and into gel phase cholesterol-free DPPC bilayers were studied in set **5** using the Slipids lipid model and ions from Refs. 6 (SD, sodium) and 7 (MK, calcium).

Finally, the binding of sodium into heterogeneous membranes with liquid ordered (L_o) and liquid disordered phases present was studied in set **6**. Here, the Slipids lipid model was used together with the ions from Ref. 6. More details on the setup of these systems is given in Section S1.2.

All membranes in sets 1–5 were built with CHARMM-GUI membrane builder [10, 11] and hydrated by 45 water molecules per lipid.

S1.2 Simulated Two-Phase System

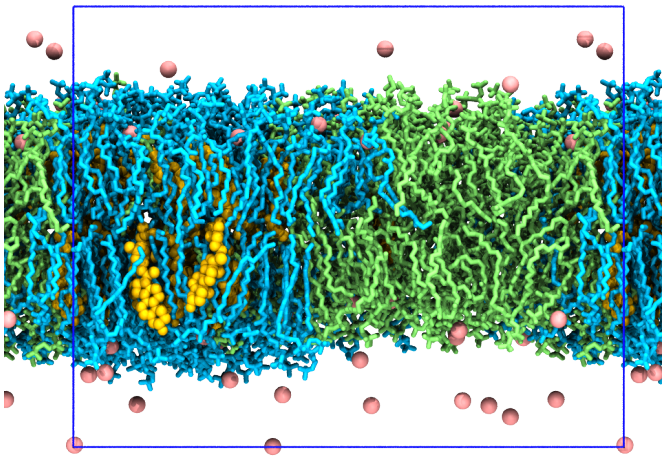

Figure S1: Side view of the ternary system consisting of DOPC (cyan), DPPC (green) and cholesterol (orange). DOPC is in the L_d phase, whereas DPPC and cholesterol together form the L_o phase. Sodium ions are shown as pink spheres. Water, lipid hydrogens and chlorides are not shown. The simulation box with periodic boundary conditions is shown in blue.

Table S1: List of simulations performed in this study (see text for explanation of "Set" numbers). The symbols correspond to initial and final bulk concentrations (c_0 and c_b), temperature (T) and simulation time (t). The used ion models are by Smith and Dang [6] (NaCl, SD), the ions with ECCR correction by Kohagen et al. [7, 12] (NaCl & $CaCl_2$, MK), the default Amber calcium parameters ($CaCl_2$, AM), and the default sodium and calcium ions in Charmm36 developed by Noskov and Roux[8] (NaCl, NR) and Marchand and Roux[9] ($CaCl_2$, MR), respectively. Note that the NBFIX correction [13] is included for Charmm36 sodium. Also note that the simulations marked with * were simulated with version 1.7 of GROMACS topology files output by Charmm-GUI, which had an issue with dihedral multiplicity. However, we expect this not to result in large changes regarding ion adsorption. The systems with no ions were rerun with fixed a topology file, and the changes in area per lipid and lipid diffusion were minor.

Set	Composition (numbers)	Salt	c_0/c_b (mM)	T (K)	FF Lipid/Ion	t (ns)
1A[14]	POPC/0% chol (200/0)	–	–/–	310	Slipids	100
	POPC/10% chol (200/22)	–	–/–	310	Slipids	100
	POPC/20% chol (200/50)	–	–/–	310	Slipids	100
	POPC/30% chol (200/86)	–	–/–	310	Slipids	100
1B[15]	POPC/0% chol (200/0)	–	–/–	310	Charmm36	100
	POPC/10% chol (200/22)	–	–/–	310	Charmm36	100
	POPC/20% chol (200/50)	–	–/–	310	Charmm36	100
	POPC/30% chol (200/86)	–	–/–	310	Charmm36	100
2A[16]	POPC/0% chol (200/0)	NaCl	130/61	310	Slipids/SD	200
	POPC/10% chol (200/22)	NaCl	130/57	310	Slipids/SD	200
	POPC/20% chol (200/50)	NaCl	130/62	310	Slipids/SD	200
	POPC/30% chol (200/86)	NaCl	130/69	310	Slipids/SD	200
2B[17]	POPC/0% chol (200/0)	NaCl	1000/703	310	Slipids/SD	200
	POPC/10% chol (200/22)	NaCl	1000/692	310	Slipids/SD	200
	POPC/20% chol (200/50)	NaCl	1000/705	310	Slipids/SD	200
	POPC/30% chol (200/86)	NaCl	1000/700	310	Slipids/SD	200
2C[18]	POPC/0% chol (200/0)	NaCl	130/84	310	Slipids/MK	200
	POPC/10% chol (200/22)	NaCl	130/87	310	Slipids/MK	200
	POPC/20% chol (200/50)	NaCl	130/85	310	Slipids/MK	200
	POPC/30% chol (200/86)	NaCl	130/90	310	Slipids/MK	200
2D*[19]	POPC/0% chol (200/0)	NaCl	130/103	310	Charmm36/NR	200
	POPC/10% chol (200/22)	NaCl	130/104	310	Charmm36/NR	200
	POPC/20% chol (200/50)	NaCl	130/105	310	Charmm36/NR	200
	POPC/30% chol (200/86)	NaCl	130/108	310	Charmm36/NR	200
3A[20]	POPC/0% chol (200/0)	$CaCl_2$	450/68	310	Slipids/MK	600
	POPC/10% chol (200/22)	$CaCl_2$	450/55	310	Slipids/MK	600
	POPC/20% chol (200/50)	$CaCl_2$	450/37	310	Slipids/MK	600
	POPC/30% chol (200/86)	$CaCl_2$	450/22	310	Slipids/MK	600
3B*[21]	POPC/0% chol (200/0)	$CaCl_2$	450/79	310	Charmm36/MK	800
	POPC/10% chol (200/22)	$CaCl_2$	450/77	310	Charmm36/MK	800
	POPC/20% chol (200/50)	$CaCl_2$	450/62	310	Charmm36/MK	800
	POPC/30% chol (200/86)	$CaCl_2$	450/61	310	Charmm36/MK	800
3C[22]	POPC/0% chol (200/0)	$CaCl_2$	450/97	310	Slipids/AM	2000
	POPC/10% chol (200/22)	$CaCl_2$	450/110	310	Slipids/AM	2000
	POPC/20% chol (200/50)	$CaCl_2$	450/99	310	Slipids/AM	2000
	POPC/30% chol (200/86)	$CaCl_2$	450/85	310	Slipids/AM	2000
3D[23]	POPC/0% chol (200/0)	$CaCl_2$	450/45	310	Charmm36/MR	2000
	POPC/10% chol (200/22)	$CaCl_2$	450/52	310	Charmm36/MR	2000
	POPC/20% chol (200/50)	$CaCl_2$	450/31	310	Charmm36/MR	2000
	POPC/30% chol (200/86)	$CaCl_2$	450/25	310	Charmm36/MR	2000
4[16, 20]	POPC (200)	NaCl	130/62	330	Slipids/SD	200
	POPC (200)	NaCl	130/56	350	Slipids/SD	200
	POPC (200)	NaCl	130/52	370	Slipids/SD	200
	POPC (200)	$CaCl_2$	450/14	330	Slipids/MK	800
	POPC (200)	$CaCl_2$	450/6	350	Slipids/MK	800
	POPC (200)	$CaCl_2$	450/2	370	Slipids/MK	800
5[24]	DOPC (200)	NaCl	130/64	310	Slipids/SD	200
	DOPC (200)	$CaCl_2$	450/25	310	Slipids/MK	500
	DPPC (200)	NaCl	130/61	295	Slipids/SD	200
	DPPC (200)	$CaCl_2$	450/130	295	Slipids/MK	800
6[24]	DOPC/DPPC/chol (166/204/52)	NaCl	150/67	310	Slipids/SD	200
	DOPC/DPPC/chol (166/204/52)	NaCl	1000/693	310	Slipids/SD	200

To further evaluate whether sodium binding depends on the phase (L_o/L_d) of the membrane, we simulated a ternary (DOPC/DPPC/cholesterol) lipid mixture with a pre-assembled phase boundary in the presence of two sodium chloride concentrations, namely 130 mM and 1 M (see Fig. S1). The ternary DOPC/DPPC/cholesterol (39%/49%/12%) system was built so that it initially contained a well-defined phase boundary separating the L_o (DPPC+cholesterol) and L_d (DOPC) phases. This boundary is stable yet it becomes slightly less sharp during the simulation. This composition is known to phase separate into coexisting liquid ordered (L_o) and liquid disordered (L_d) phases in experiments [25]. Two NaCl concentrations, namely ∼150 mM and ∼1 M were employed. The Slipids force field [1–3] was employed together with the ion parameters of Smith and Dang [6].

S1.3 Simulation Parameters

S1.3.1 Simulations With the Slipids Force Field

The membranes were simulated in the NPT ensemble at 1 bar using the velocity rescaling thermostat [26] and a semi-isotropic Parrinello–Rahman barostat [27]. Their time constants were set to 0.5 and 1 ps, respectively. The temperatures of the membrane and the solvent were coupled separately. Constraints were applied to all bonds using the Lincs algorithm [28].

The smooth PME scheme [29, 30] was employed for the electrostatics, whereas the Lennard-Jones (LJ) potential was cut off at 1 nm. To account for the long-range LJ interaction, dispersion correction was applied to both energy and pressure. A neighbor list with a radius of 1 nm was updated every 10 steps.

The simulations, varying in length (see Table S1), were all performed with a time step of 2 fs employing the GROMACS v4.6.x [31] simulation package.

S1.3.2 Simulations With the Charmm36 Force Field

The simulations using the Charmm36 force field were performed with the simulation parameters provided by the CHARMM-GUI. Namely, the NPT ensemble was provided by the Nóse–Hoover thermostat [32, 33] and the Parrinello–Rahman barostat [27]. The time constats were set to 1 and 5 ps for the thermostat and barostat, respectively. The bonds connected to hydrogen atoms were constrained with the Lincs algorithm [28]. The smooth PME scheme [29, 30] was employed for electrostatics. The LJ interactions were cut off at 1.2 nm and the force switch modifier was employed from 1.0 nm on. The Verlet-type neighbor list was employed. The simulations were performed using a 2 fs integration time step using the GROMACS v.5.0.x [34] simulation package.

S1.4 Analysis Methods

All analysis was performed using either the last 50 ns (systems without ions), the last 150 ns (systems containing sodium) or the last 250 ns (systems containing calcium) of the data. Membrane areas and numbers of contacts and were calculated with `g_energy` and `g_mindist` tools bundled with GROMACS, respectively. A cation within 0.325 nm from a lipid oxygen was defined to be bound to the membrane. This definition was carefully validated, see Section S1.4.1. The dynamic surfaces, employed as an alternative criterion for bound ions (see below), were calculated with `g_lomepro` [35] and processed with MATLAB [36].

Diffusion coefficients (D) were extracted by a linear fit ($\mathrm{MSD} = 4D\Delta$) to the lag time (Δ) interval between 10 and 30 ns of the mean squared displacement (MSD) data, calculated from the center of mass trajectory (generated by `g_traj`) with the `g_msd` tool. Lipid motion was measured with respect to the centre of mass of the bilayer, hence bilayer drift does not affect the diffusion coefficients.

S1.4.1 Ion Binding and Coordination Cut-Offs Do Not Affect the Results

In this work, an ion was defined to be bound to the membrane if it was closer than 0.325 nm from any oxygen atom of the phospholipid. This definition was chosen so that the number of possible binding sites would be constant regardless of the number of cholesterol concentration. We also carefully validated that this definition does not affect the results in two ways.

First, we included the cholesterol oxygens in the analysis. The values obtained this way for sodium are shown (blue curve) in Fig. S2 together with those obtained by only considering PC oxygens (red curve). The contacts between calciums and cholesterol hydroxyl oxygens are also very rare (data not shown).

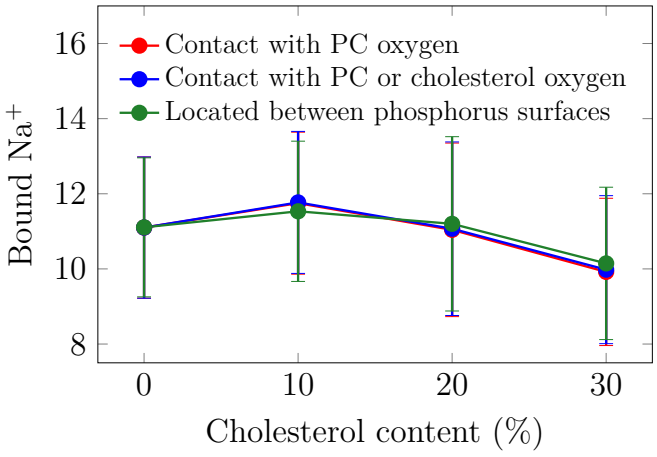

Figure S2: The number of bound sodiums determined in three ways. Average number of sodiums that are closer than 0.325 nm to a PC oxygen are shown in red. Similarly, the average number of sodiums that are closer than 0.325 nm to either a PC or cholesterol oxygen are shown in blue. The average number of sodium ions located between dynamic surfaces defined by phosphorus positions (see text) is shown in green. Error bars show standard deviations.

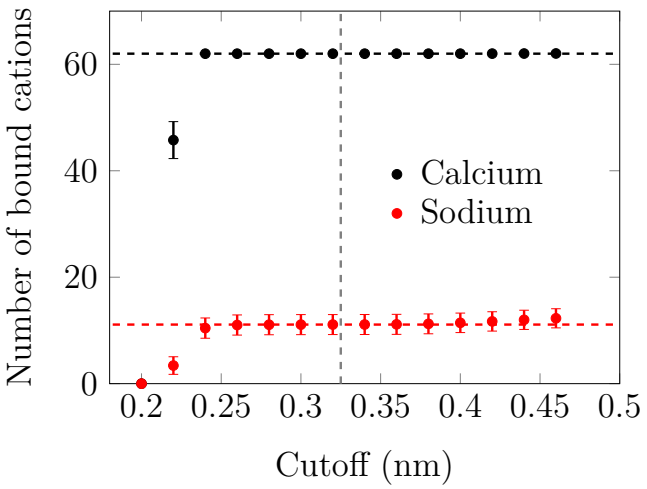

Figure S3: Number of bound ions as a function of the cutoff length for both sodium and calcium ions. The employed value as well as the number of bound ions measured with this value are highlighted with dashed lines. The cholesterol-free membrane and the Slipids lipid model were employed together with the sodium model of Smith and Dang (SD) and the ECCR corrected calcium model (MK).

Second, we also evaluated the number of bound ions based on their location with respect to the membrane surface. Since even membranes formed of 200 lipids fluctuate slightly, density profiles do not necessarily provide a good estimate of bound ions. Instead, we calculated the number of ions that are located between two surfaces that are defined as follows: First, continuous surfaces are generated through interpolation from the phosphorus atom locations. Then, these surfaces are extended 0.3 nm outwards from the membrane core.

This definition takes into account all oxygens that are bound to the phosphate oxygens. The ion positions are recorded every nanosecond and the surfaces are generated from the average positions of the phosphorus atoms during this nanosecond interval. The analysis is therefore repeated for every nanosecond of data. The number of bound sodiums calculated this way is also shown in Fig. S2 (green curve). This curve agrees substantially well with those obtained using the two other definitions.

Finally, we also calculated the number of bound ions with different cutoff lengths (in addition to the employed 0.325 nm). As shown in Fig. S3, the number of bound ions is very insensitive to the choice of the cutoff length for both sodium and calcium.

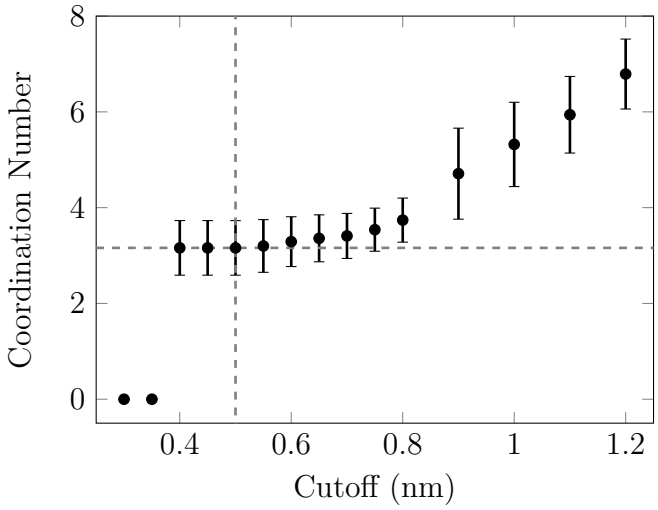

Figure S4: The effect of cutoff on the average coordination number (phosphori) of calcium ions. The cholesterol-free POPC bilayer using Slipids lipid force field and the ECCR corrected ions (MK) is employed.

When calculating coordination numbers of calcium bound to a bilayer, phosphori closer than 0.5 nm from a calcium ion are considered to be in contact with it. As shown in Fig. S4, the coordination numbers are also not sensitive to the change of this cutoff length.

These results together clearly support the robustness of the used definitions.

S2 Fluorescence Methods

S2.1 Materials

1-palmitoyl,2-dioleoyl-*sn*-glycero-3-phosphocholine (POPC) and ovine wool cholesterol were purchased from Avanti Polar Lipids, Inc. (Alabaster, USA). 6-lauroyl-2-dimethylaminonaphthalene (Laurdan) was obtained from Molecular Probes (Eugene, USA). Calcium chloride and sodium chloride with purity $\geq$ 99% and ethylenediaminetetraacetic acid (EDTA) were purchased from Sigma-Aldrich (St. Louis, USA). Organic solvents of spectroscopic grade were supplied by Merck (Darmstadt, Germany). All chemicals were used without further purification.

S2.2 Liposome Preparation

Appropriate volumes of lipids and Laurdan stock solutions were mixed in glass tubes. The final lipid concentrations were 1.0 mM for pure POPC and 1.25 mM for POPC/Chol liposomes. Consequently, the concentration of POPC was kept constant between the samples as in MD simulations. The final Laurdan concentration was 0.01 mM in all the samples. Mixtures were dried under nitrogen stream and left for at least 2 hours in vacuum. Dry lipid film was rehydrated in 1.5 mL sterile-filtered water (Sigma-Aldrich, St. Louis, USA) containing either 0.1 mM EDTA or appropriate concentration of salt and vortexed for 4 mins.

Large unilamellar vesicles (LUVs) were formed by extrusion through a 100 nm pore diameter membrane filters (Avestin, Ottawa, Canada).

S2.3 Fluorescence Measurements

All measurements were performed in 1.5 mL quartz cuvettes (Hellma, Müllheim, Germany) thermostated at 288 K, 298 K, or 310 K using water circulating bath. Steady-state emission and excitation spectra were recorded on a Fluorolog-3 spectrofluorometer (model FL3–11; JobinYvon Inc., Edison, NJ, USA) equipped with a xenon-arc lamp. Excitation generalized polarization (GP_{EX}) was calculated from excitation spectra measured for the emission at 440 and 490 nm in the range 340–380 nm, according to: $GP_{\mathrm{EX}} = (I_{440} - I_{490})/(I_{440} + I_{490})$, where I_{440} and I_{490} are the mean fluorescence intensities emitted at 440 and 490 nm [37].

Time-resolved fluorescence was recorded using a 5000U Single Photon Counting setup equipped with a cooled Hamamatsu R3809U-50 microchannel plate photomultiplier (IBH, UK). Emission >399 nm cutoff filter was used to eliminate the scattered light. Laurdan probe was excited at 373 nm with the IBH NanoLed 11 laser diode and fluorescent decays were collected between 400 and 540 nm with a 10 nm step. Each decay was fitted with a multi-exponential function using the iterative reconvolution procedure (IBH DAS6 software). Time-Resolved Emission Spectra (TRES) were reconstructed from the decays and the steady-state emission spectrum and fitted with log–normal function in order to determine position of their maxima, $\nu(t)$, and their width[38]. Subsequently, $\nu(t)$ was used to calculate mean relaxation time and total emission shift ($\Delta\nu$).

The relaxation times were integrated after first normalizing them in the form of correlation functions $C(t)$ with $C(0) = 1$ and $C(T) = 0$, where T is 15 ns and 30 ns for measurements at 310 K and 298 K, respectively. These curves were then integrated from 0 to T to get an average relaxation time. This approach was not suitable for the measurements at 288 K. For them, the mean relaxation time, τ_r, was obtained by the fitting of two-exponential function: $\nu = \nu_0 + A_1 \exp(-t/\tau_1) + A_2 \exp(-t/\tau_2)$ to the measured $\nu(t)$, and averaging the obtained decay constants: $\tau_r = (A_1\tau_1^2 + A_2\tau_2^2)/(A_1\tau_1 + A_2\tau_2)$. The total emission shift was calculated, as $\Delta\nu = \nu(0) - \nu(\infty)$, where $\nu(0)$ and $\nu(\infty)$ are TRES positions before and after dipolar relaxation, respectively. $\nu(0)$ was estimated according to Ref. 39 to be 23800 cm^{-1} for Laurdan. Intrinsic uncertainties are 0.05 ns for τ_r and 50 cm^{-1} for $\Delta\nu$.

S2.4 Excitation Generalized Polarization

In excitation generalized polarization (GP_{EX}) the emission maxima at 440 and 490 nm are phenomenologically assigned to the gel and liquid crystalline lipid phases, respectively [37]. GP_{EX} values ranging from about -0.4 for liquid disordered (L_d) to $+0.6$ for gel phases provide a rough measure of the changes in the local lipid hydration or packing.

S3 Additional Experimental Results

S3.1 Generalized Polarization Measurements (GP_{EX})

Generalized polarization measurements, shown in Fig. S5, reveal that both the addition of cholesterol or the decrease in the temperature apparently increase the ordering in the system. Interestingly, the decrease of temperature by 22 K from 310 K to 288 K induces a larger increase in GP_{EX} than the addition of 20% cholesterol. This suggests that when lowering the temperature we do not only witness changes in membrane packing, but also the slowdown of the self diffusion of Laurdan, which amplifies the observed variations. Considering now the interaction of these membranes with Ca^{2+} and Na^{+}, we see a linear increase in the calculated GP_{EX} values with an increasing salt concentration. This effect is significantly larger for $CaCl_2$ than for NaCl, independently of the temperature and the presence of cholesterol. The slopes of the linear fits presented in Fig. S5 range from 0.01–0.05 M^{-1} for NaCl to 0.08–0.20 M^{-1} for $CaCl_2$. In fact, adding NaCl has virtually no effect on GP_{EX}, in other words on the membrane environment surrounding Laurdan. In contrast, Ca^{2+} has a clear albeit rather complex effect on GP_{EX} for both concentrations (150 mM and 1.0 M). As GP_{EX} contains convoluted information on the polarization of the environment as well as on the packing/local mobility, the TDFS method is required to deconvolute the result into the two contributions. The results obtained with the TDFS method are shown in the main text and in S3.2.

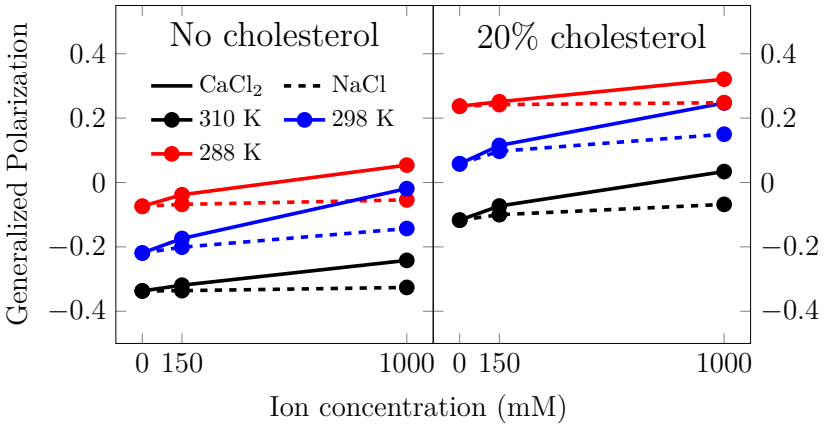

Figure S5: Generalized polarization measurements.

S3.2 Time-Dependent Fluorescence-Shift Measurements (TDFS)

Examples of the $\nu(t)$ relaxation curves are shown in Fig. S6 for the POPC and POPC/20% chol systems at 298 K, both on semi-logarithmic and linear axes. The relaxation time τ_r as a function of cholesterol content, temperature, and ionic environment is shown in Fig. S7. Whereas data for 310 K were shown in the main text, data for two other measured temperatures (288 K and 298 K) are shown here.

It might seem possible that the direct ion–Laurdan interactions could explain the increased relaxation times. However, this possibility seems unlikely based on the local polarization measurement provided also by TDFS, shown in Fig. S8. We observe that the polarity of the environment of Laurdan does not change substantially in our experiments with all measurements falling within the error range. The simulations also show similar behavior, see Section S4.4. This indicates that the Laurdan–solution interaction is negligible, in accordance with the positioning of Laurdan below the *sn*-1 carbonyl [40] where polarizability of the environment is rather low due to the scarcity of water present. Otherwise, the dehydration observed at the membrane surface upon the addition of cholesterol [41] would affect local polarization. For the same reason no changes are observed with increasing ion concentration, suggesting that no direct ion–Laurdan interaction exists. This evidences the inability of ions to insert below the carbonyl level in the membrane. It is also clear that the changes observed in GP_{EX} (see Fig. S5) are solely due to changes in Laurdan relaxation times and not in its hydration.

Note that $\Delta\nu$ data for the POPC/Chol mixture could not be measured at 288 K or at 298 K.

S4 Additional Computational Results

S4.1 Sodium Binding Is Not Affected by the Membrane Phase

The number of sodium ions bound to the L_o phase (16.9) is ∼24% higher than that in the L_d phase (13.6) with 130 mM NaCl, respectively. At first, this observation seems to be in direct disagreement with the results recently reported in Ref. 42 where apparently the presence of cholesterol was found to lead to less sodium adsorption. However, while these two phases have the same area, the number of PC head groups in the L_o phase (204) is ∼23% larger than that in the L_d phase (166). Hence, when the numbers of bound ions in the two phases with equal area are normalized by the by the number of PC lipids present in them, no significant difference between the two phases is observed, as shown in Fig. S9. This follows the observations presented in the main paper for single phase bilayers and agrees with the result in Fig. S9 of Ref [42]. This result also holds for a 1 M concentration of NaCl, where the number of sodium ions bound to the L_o phase (69.5) is ∼27% higher than that in the L_d phase (54.9), as demonstrated in Fig. S9.

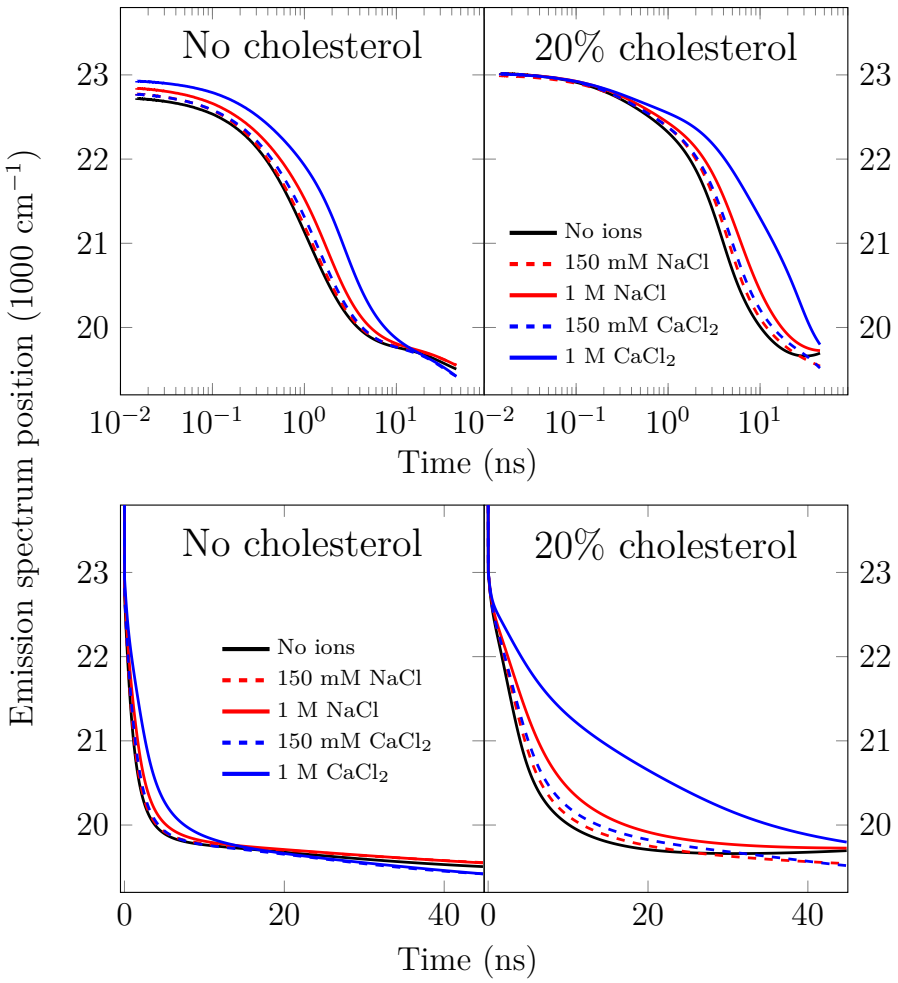

Figure S6: Relaxation curves from time-dependent fluorescence-shift measurements performed at 298 K. Data is shown on both semi-logarithmic (top row) and linear (bottom row) axes.

S4.2 Effect of Temperature on Cation Binding Is Complex

Figs. S10 and extend the figures shown in the main paper by including the simulations on POPC bilayers performed at higher temperatures. These elevated temperatures, equal to 330 K, 350 K, and 370 K, are shown in blue with the area per PC systematically increasing upon temperature increase. The system simulated at 310 K is shown in blue/red, since it belongs to the two data sets.

It is evident that the results obtained at higher temperatures deviate somewhat from the behavior of other systems suggesting that in addition to the relations resolved in the main paper, namely the the number of PC head groups and the membrane area, other and more complex factors are in play.

S4.3 Rotational Freedom of Cholesterol Resembles That of Laurdan

Since our simulations do not contain Laurdan, we use the rotational autocorrelation function of cholesterol to roughly estimate how the increase of cholesterol and salt concentration could affect the rotational diffusion of Laurdan. This is justified by the similar size and positioning of Laurdan and cholesterol in the membrane. The cholesterol vector used to calculate the ACF_{ROT} is the one between atoms C13 and C18 following Ref. 43. From the decay curves extracted from simulations, shown in Fig. S11, one can extract the relaxation times shown in Fig. S12 by fitting a double exponential function. The same formula for extracting the relaxation

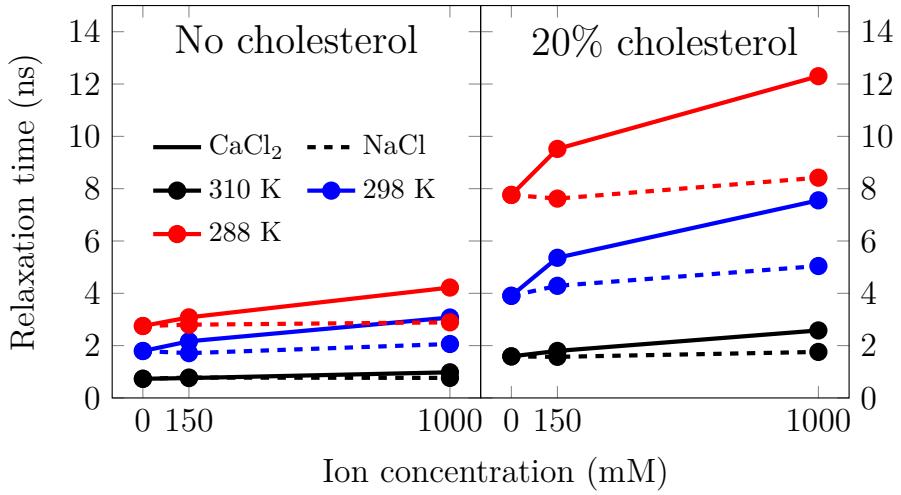

Figure S7: Relaxation times from time-dependent fluorescence-shift measurements for all three measured temperatures.

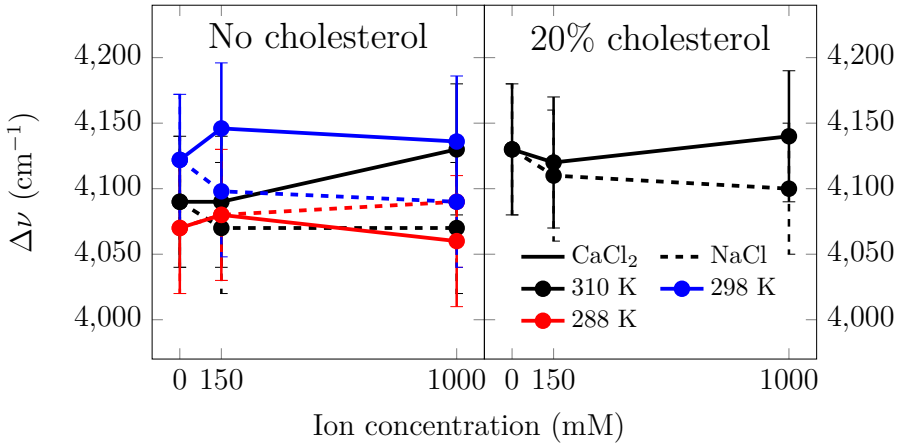

Figure S8: $\Delta\nu$ from time-dependent fluorescence-shift measurements.

time τ_r as for the Laurdan experiments, given in the main text, is used.

S4.4 Hydration of Cholesterol Is Not Affected by Ions

In our experiments, we did not observe a significant change in polarity, characterized by $\Delta\nu$, upon the addition of cholesterol or ions as shown in Fig. S8. This suggests that the hydration of Laurdan is not affected by these changes. Analysis on the hydration of cholesterol hydroxyl group, residing in the same carbonyl region as Laurdan, confirms these findings. As shown in Fig. S13, the hydration levels are not significantly affected by either the addition of ions or cholesterol.

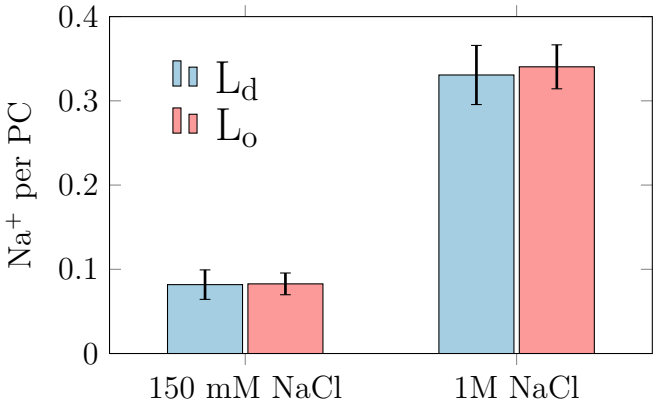

Figure S9: Number of bound sodium ions per PC head group in the two-phase (L_o/L_d) system. Error bars show standard deviation.

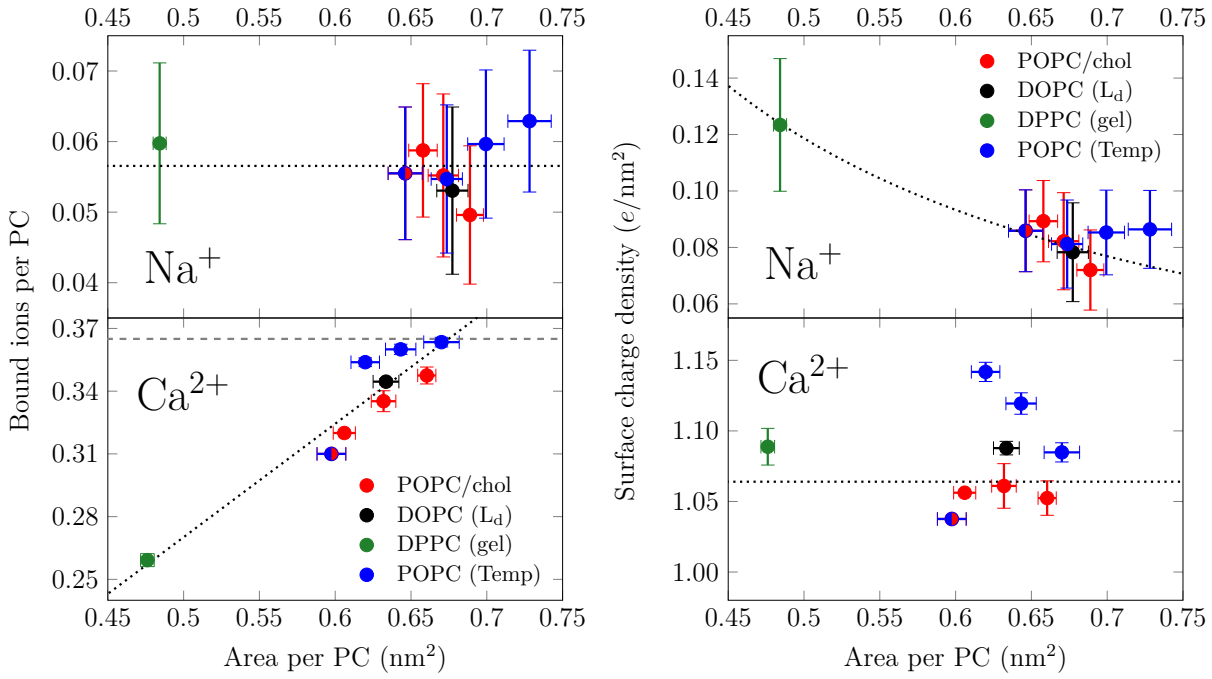

Figure S10: The dependence of cation adsorption on the area per phospholipid (Left). The dependence of cation charge density on the area per phospholipid in membranes (Right). In addition to the data shown in the main paper, data for elevated temperatures is shown. Red dots are POPC with 10, 20, or 30% cholesterol at 310 K (smallest to highest area). Black dot is DOPC at 310 K. Green dot is DPPC at 295 K. Blue dots are POPC at 330 K, 350 K, and 370 K (smallest to highest area. The red/blue dot is 0% cholesterol at 310 K, hence it belongs to two data sets. Error bars show standard deviation.

S5 Computational Results Are Independent of the Employed Models

This section characterizes in detail the binding of ions to membranes in our simulations and describes numerous small and large differences in the behavior of the tested lipid and ion force fields. Small differences

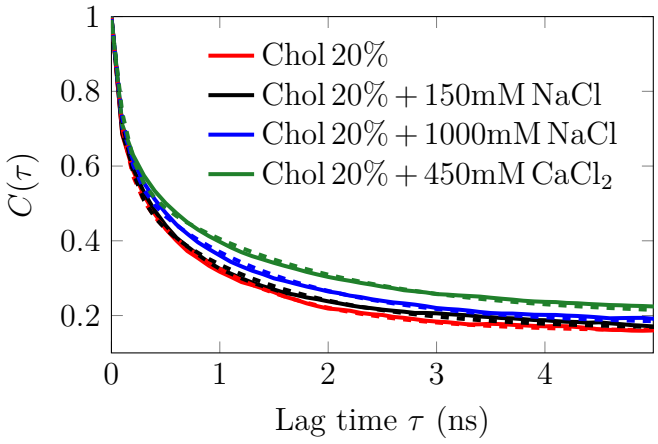

Figure S11: ACF_{ROT} of cholesterol as a function of salt concentration in the simulations. A double exponential fits are also shown with dashed lines.

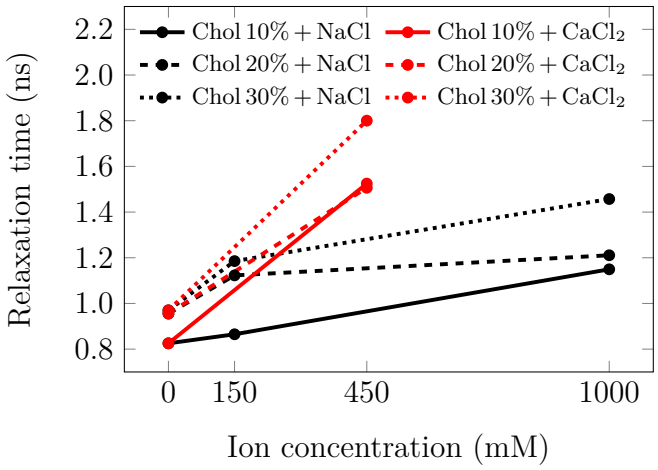

Figure S12: Relaxation time τ_r of cholesterol rotation as a function of salt concentration in the simulations.

are seen in the ability to condense lipid bilayers and to affect lipid diffusion, as well as in coordination numbers of bound calcium ions. Larger differences, on the other hand, are seen in the binding mode of both the calcium and sodium ions. However, despite these features, the key results presented in the main text are consistently reproduced across all employed models.

S5.1 Ion Binding Results in Tighter Phospholipid Packing

The area per POPC molecule is plotted in Fig. S14 as a function of cholesterol content. The effect of ions is evident in this figure. Whereas the effect of small concentration (130 mM) of weakly-binding sodium is fairly small, a larger concentration (1 M) decreases the area per POPC by approximately 3 $Å^2$. An even stronger effect is observed for a concentration of 450 mM of calcium, and the models with full charge (AM and MR) result in smallest areas per lipid.

In addition to condensing the bilayers, ions also affect lipid mobility. As shown in Fig. S15, calcium ions drastically slow down the diffusion of POPC whereas sodium has no effect, in line with their effect on area per PC (see Fig. S14) and relaxation times probed by Laurdan. Addition of cholesterol consistently slows down lipid diffusion, as expected.

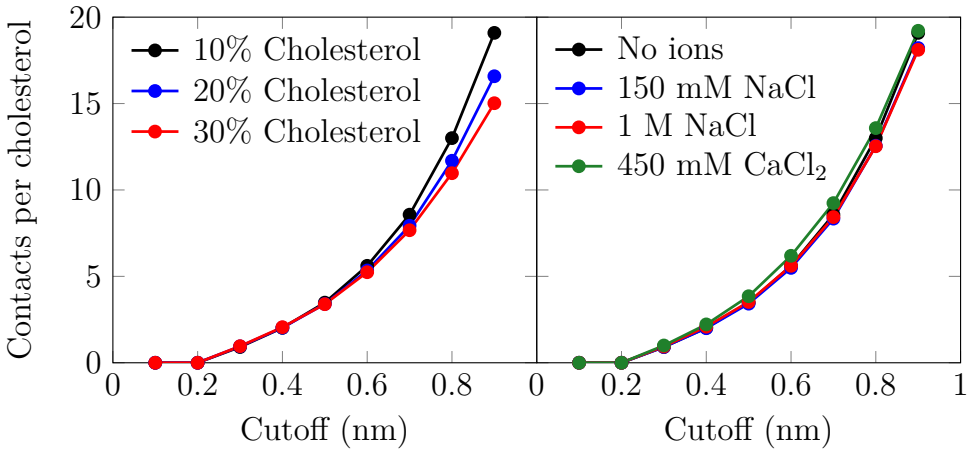

Figure S13: Hydration of cholesterol hydroxyl group. Number of water molecules within a cutoff from the hydroxyl group are shown as a function of cholesterol concentration as well as ion type and concentration.

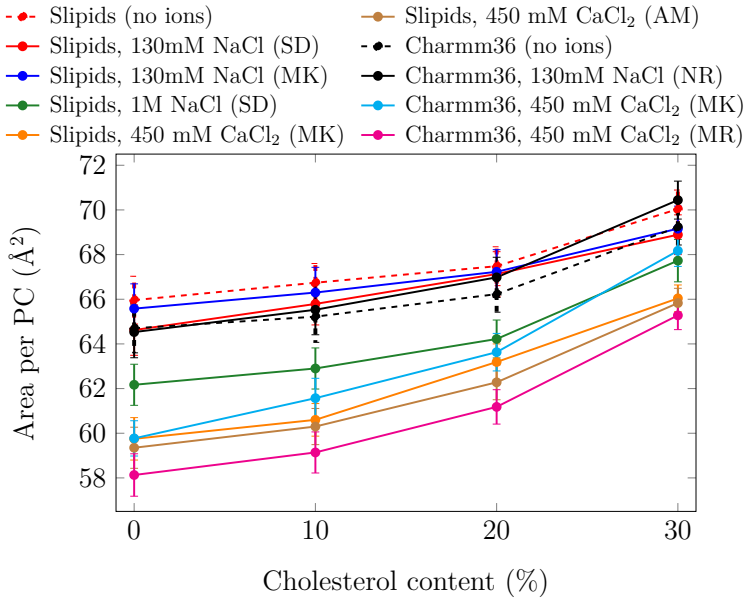

Figure S14: Dependence of area per POPC molecule on the inclusion of cholesterol when exposed to sodium or calcium. Error bars show standard deviations.

S5.2 Effect of Cholesterol on Ion Binding Is Consistent Among Tested Models

The number of bound ions versus cholesterol content is shown in Fig. S16 for the Charmm36 lipid model [4, 5] and for its default ion model [8] with the NBFIX correction [13]. Also data for Slipids [1–3] with the recent sodium chloride parameters [7] are shown in Fig. S16. The data shown in the main text is also included in the figure for better comparison between the models.

In the main text, adsorption of sodium to a POPC membrane was shown to not depend on the presence of cholesterol and this is also verified with Charmm36. Additionally, the increase in calcium binding due to the increase in cholesterol content reported in the main text is also reproducible with Charmm36 lipids and the ion model employing the ECCR correction [7]. Furthermore, the behavior of both Slipids and Charmm36 lipids with their standard ion models is also consistent with this observation yet the effect seems to be

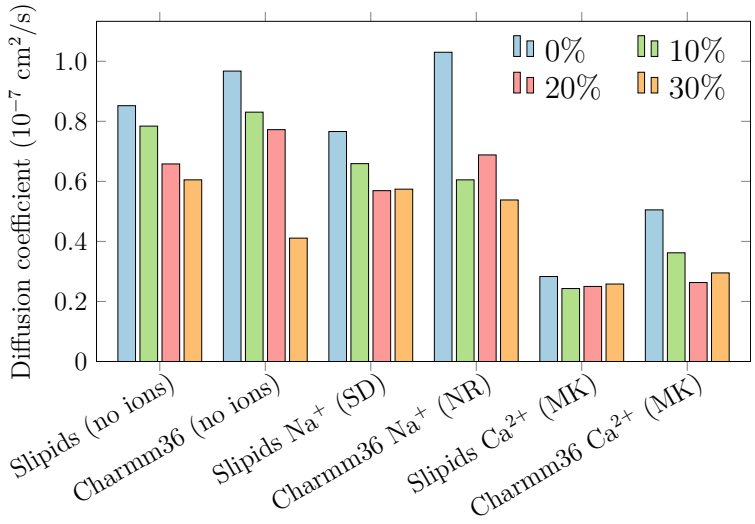

Figure S15: Effect of ions on the diffusion coefficients of POPC.

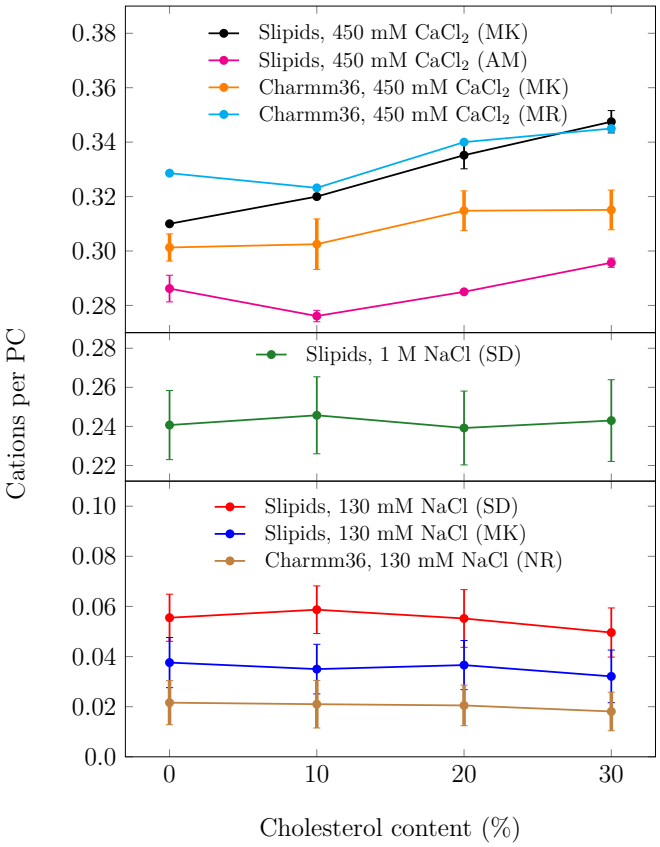

Figure S16: Effect of cholesterol on the number of bound ions showed in the main text is also reproduced with other lipid and ion models.

somewhat smaller (see Fig. S16).

S5.3 Membrane Surface Saturates with Calcium

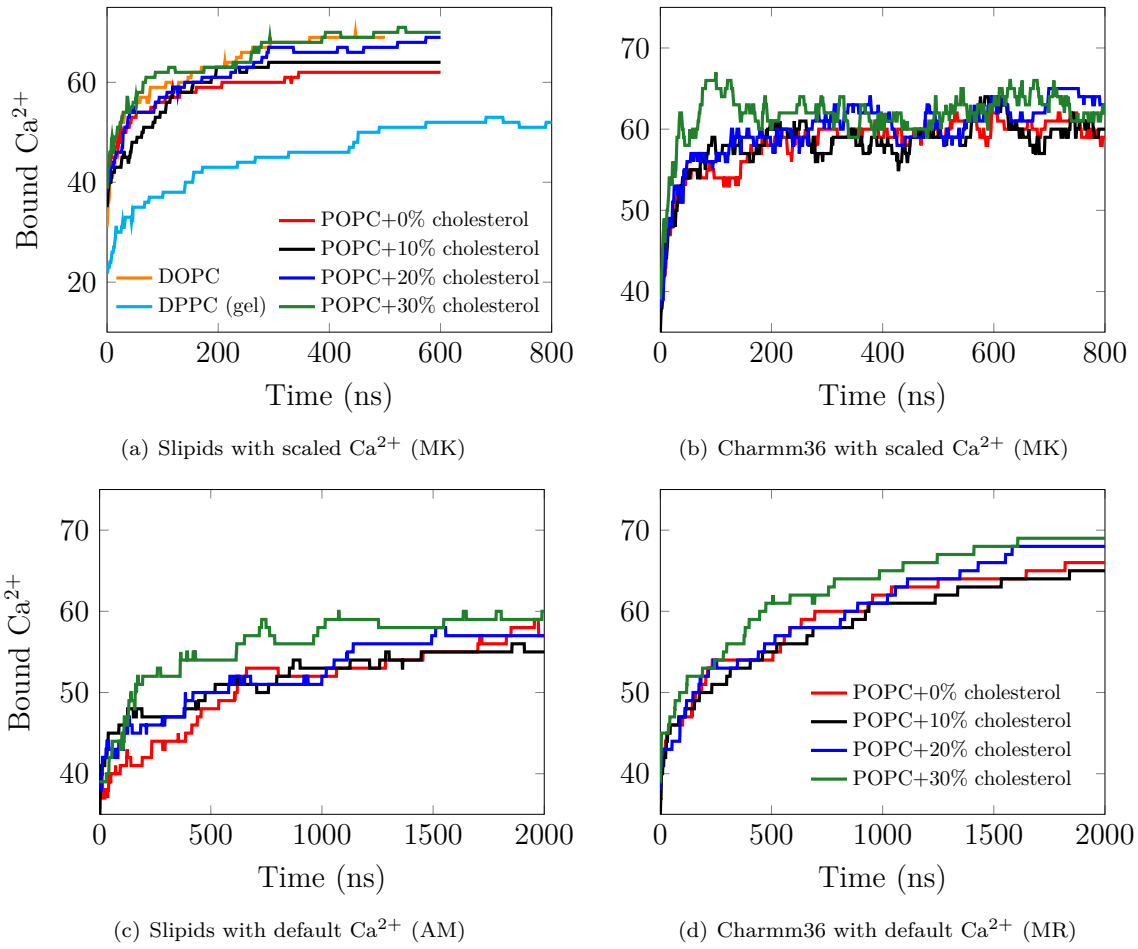

(a) Slipids with scaled Ca^{2+} (MK)

(b) Charmm36 with scaled Ca^{2+} (MK)

(c) Slipids with default Ca^{2+} (AM)

(d) Charmm36 with default Ca^{2+} (MR)

Figure S17: The number of adsorbed calcium ions versus time in a number of systems with different lipid and ion models. Last 250 ns of these simulations are employed in all analyses.

Sodium ions exchange constantly between the membrane surface and the bulk water, which means that the systems containing sodium ions reach equilibrium fairly quickly. To ensure that the simulations with calcium have reached equilibrium, we verified that the number of bound calcium ions did not show any drift during the last 250 ns (employed for analyses) of the simulations. Indeed, as shown in Fig. S17, the number of bound calcium ions eventually reaches a plateau in all systems, even though this takes more time in the gel-phase DPPC bilayer or in systems simulated with the calcium models with a charge of +2 (AM and MR).

S5.4 Calcium Ions Simultaneously Bind to Three Lipids

Calcium adsorbs rapidly into the membrane and generates characteristic complexes with lipids. These complexes are visualized in Fig. S18, where the calcium positions are plotted at the end of selected simulations together with the phosphorus atoms. Phosphori and bound ions are shown for one leaflet. Data are shown for both Slipids [1–3] and Charmm36 [4, 5] lipid force fields and for the ion model that takes the polarization into account in an effective way [7]. Data are shown for systems with 0% and 30% cholesterol. In the latter case, the positions of cholesterol hydroxyl oxygens are also drawn.

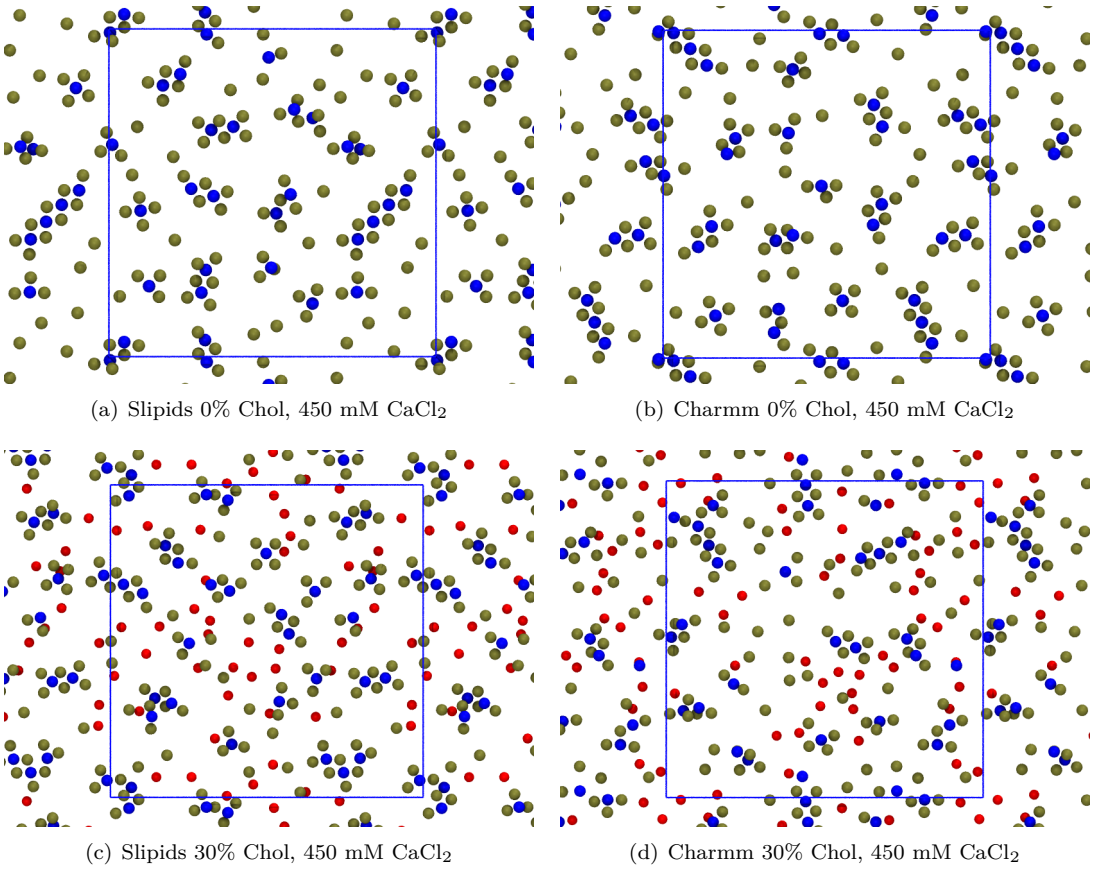

(a) Slipids 0% Chol, 450 mM $CaCl_2$

(b) Charmm 0% Chol, 450 mM $CaCl_2$

(c) Slipids 30% Chol, 450 mM $CaCl_2$

(d) Charmm 30% Chol, 450 mM $CaCl_2$

Figure S18: Snapshots of the positions of phosphorus atoms (brown), calciums (blue) and cholesterol oxygens (red) of one leaflet at the end of the simulation. Very stable clusters containing calciums and phosphori in the 1:3 ratio are observed. Cholesterol seems not to play a role in the formation of these clusters.

From Figs. 18(a) and 18(b) it seems that bound calciums are coordinated with 3 phosphori in the cholesterol-free systems, whereas the situation is not that clear in the cholesterol-containing systems (Figs. 18(c) and 18(d)).

This coordination with 3 phosphori is also evidenced by Fig. S19, which shows the average number of phosphorus contacts for a calcium ion adsorbed to the membrane surface.

A more thorough investigation reveals a fairly wide distribution of coordination numbers. These distributions, shown in Fig. S20 for the ECCR corrected ions (MK) and for both Slipids and Charmm36 force fields, reveal that some ions are coordinated to an average of 4 phosphori, whereas 3 is the most common coordination number.

Based on this analysis, the addition of cholesterol does not have a large effect on the calcium–phosphate coordination, and the coordination number is close to 3 even in the gel phase. Interestingly, the values increase when a cholesterol-free POPC membrane is heated up. This probably results from the greater adaptability of the lipid head groups to the bound calcium due to their increased flexibility.

S5.5 Density Profiles Reveal Differences Between the Models

The density profiles also confirm that the number of sodium ions interacting with the membrane does not change upon addition of cholesterol. Additionally, they reveal the different behavior among the studied models. These profiles are plotted for different cholesterol concentrations and for different models in Fig. S21. All plots are aligned so that the maxima of the phosphorus density in each system is located at the same position.

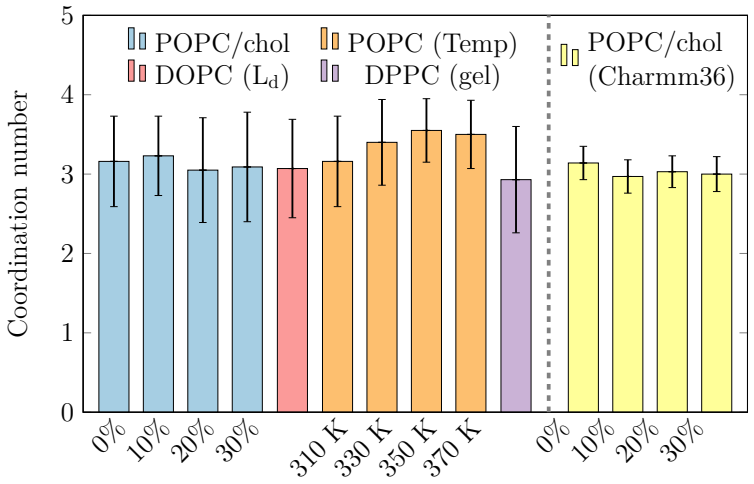

Figure S19: Average number of phosphorus atoms that are within 0.5 nm of a bound calcium ion in various studied systems.

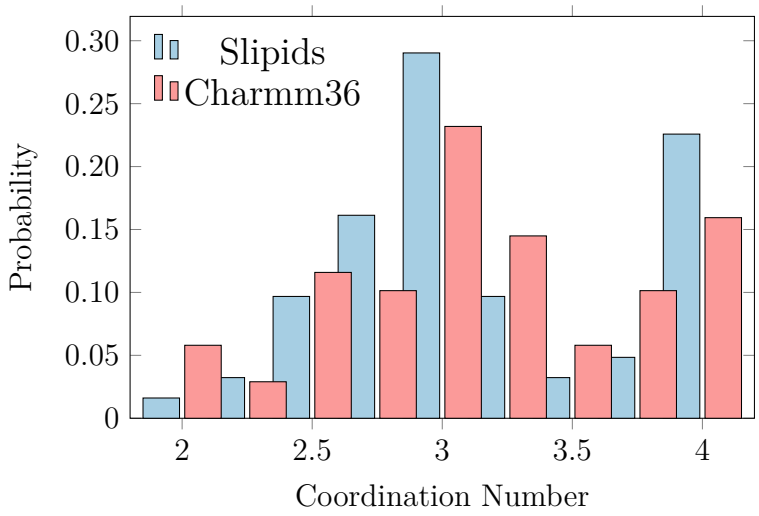

Figure S20: The probabilities of various coordination numbers for cholesterol-free bilayers shown for the Slipids and Charmm36 lipid models with the ECCR-scaled ions (MK).

Whereas the ion model (SD) by Smith and Dang together with the Slipids provides a 2.5-fold increase of sodium concentration in the membrane surface as compared to the bulk water (see Fig. 21(a), this difference is reduced to 1.5-fold when the ion model with effective polarization by Kohagen et al. (MK) is employed instead (see Fig. 21(b)). These correspond to binding free energies of ∼2.4 and ∼1 kJ/mol, respectively. As a comparison, GROMOS force field suggests a much higher accumulation (6-fold increase [44], corresponding to binding free energy of 4.6 kJ/mol) of sodium on the surface of a PC membrane. As shown in Fig. 21(c), density profiles for Charmm36 lipid force field together with its default ion model by Noskov and Roux does not provide a maximum in the density profile at the membrane head group region due to the extra repulsion between sodium and the lipid oxygens [13]. Notably, even with this fix, an approximately 1.5-fold increase in sodium concentration at the membrane surface as compared to the bulk water has been measured [44]. In the case of Slipids and 1 M of sodium (SD), the density of sodium at the membrane surface is similar to that in the bulk water (see Fig. 21(d)). These two are separated by a noticeable minimum occupied by chlorides.

The density profiles for calcium ions are shown in Fig. S22. The curves using Slipids and Charmm36 lipid models show very similar behavior when both are combined with the calcium model with effective polarization (MK). Importantly, the height of the density maxima grow upon addition of cholesterol in line with the increased number of adsorbed ions. The density profiles also suggest that the adsorption is strongest for the Charmm36 lipid model combined with its standard calcium parameters with full charge (MR).

S5.6 Cations Interact Mostly With Phosphate Oxygens

To define which lipid oxygen atoms are involved in the adsorption of sodium and calcium into membranes, we calculated separately the number of ion contacts formed by phosphate and ester oxygens. These preferential binding sites are shown in Fig. S23 for selected model combinations and for the cholesterol-free POPC membranes.

These plots suggest that with the Slipids lipid model, sodium interacts preferentially with the phosphate oxygens, whereas with Charmm36 lipids they prefer the ester oxygens. However, the differences are small in line with the observed weak binding and rapid exchange of ions between the bilayer and the aqueous phase.

Calcium, on the other hand, clearly prefers to attach to the phosphate oxygens with both lipid models and both ion models. For the model with effective polarization (MK), the binding modes of Slipids and Charmm36 lipid models are very similar with phosphate oxygens binding approximately twice as many calcium ions as the carbonyl ester oxygens. However, for the calcium models with full charge (sets 3C and 3D in Table. S1), the lipid models behave differently. Combined with Slipids, these ions penetrate deep so that ∼70% of them also interact with carbonyl ester oxygens. Combined with Charmm36, on the other hand, the ions with full charge form very few contacts with ester oxygens ($< 5\%$ of bound ions). Notably, this deeper penetration with the Slipids model is also highlighted by the density profiles shown in Figs. S22(c) and S22(d).

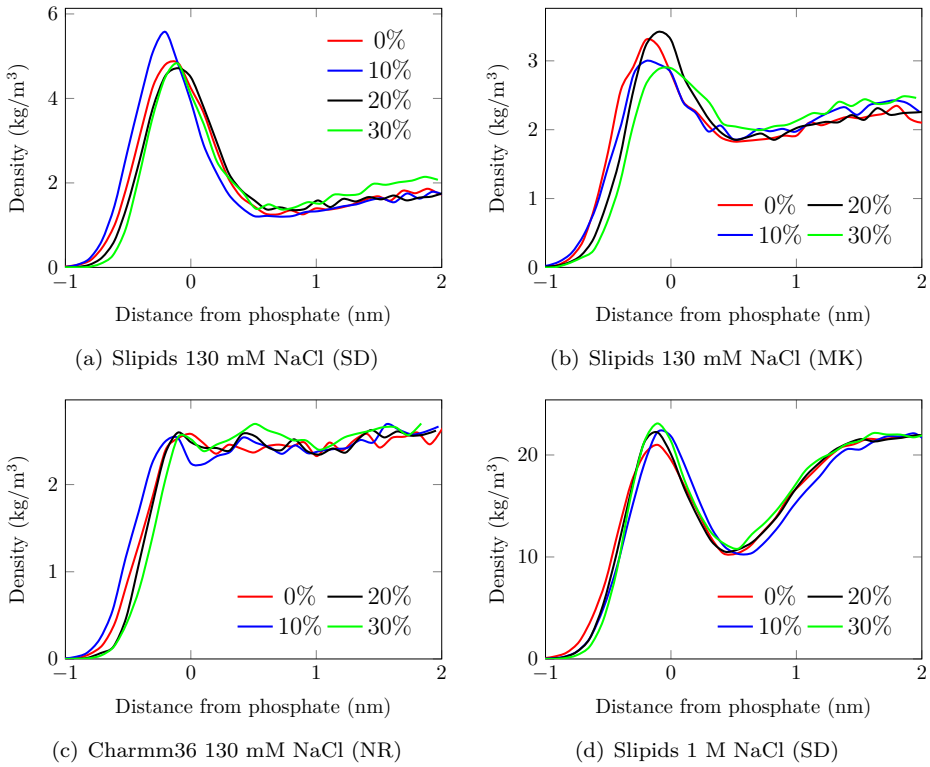

(a) Slipids 130 mM NaCl (SD)

(b) Slipids 130 mM NaCl (MK)

(c) Charmm36 130 mM NaCl (NR)

(d) Slipids 1 M NaCl (SD)

Figure S21: Density profiles of sodiums aligned based on the maxima of the phosphate density. The behavior of the models is very different yet the changes induced by cholesterol are minimal in all models.

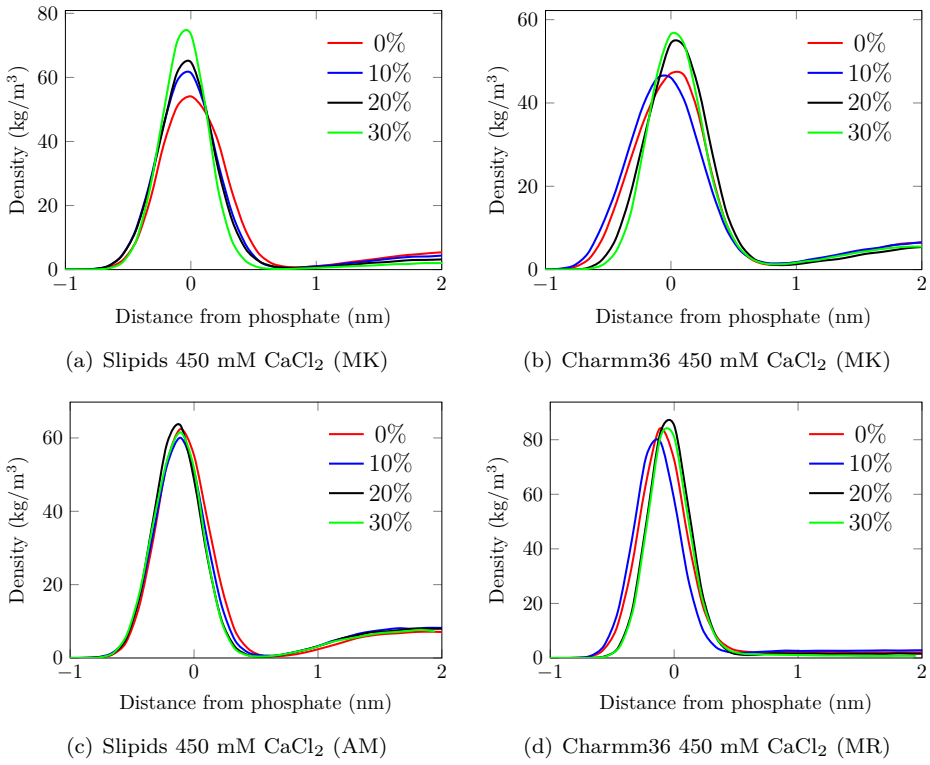

(a) Slipids 450 mM $CaCl_2$ (MK)

(b) Charmm36 450 mM $CaCl_2$ (MK)

(c) Slipids 450 mM $CaCl_2$ (AM)

(d) Charmm36 450 mM $CaCl_2$ (MR)

Figure S22: Density profiles of calciums aligned based on the maxima of the phosphate density. The two lipid force fields together with two ion force fields each behave in a fairly similar way. However, for the scaled ions, Slipids binding is increased more upon addition of cholesterol. In Charmm36 with scaled ions this effect is present but more subtle. With the standard calcium models of the Amber (Slipids) and Charmm36, the behavior is reversed.

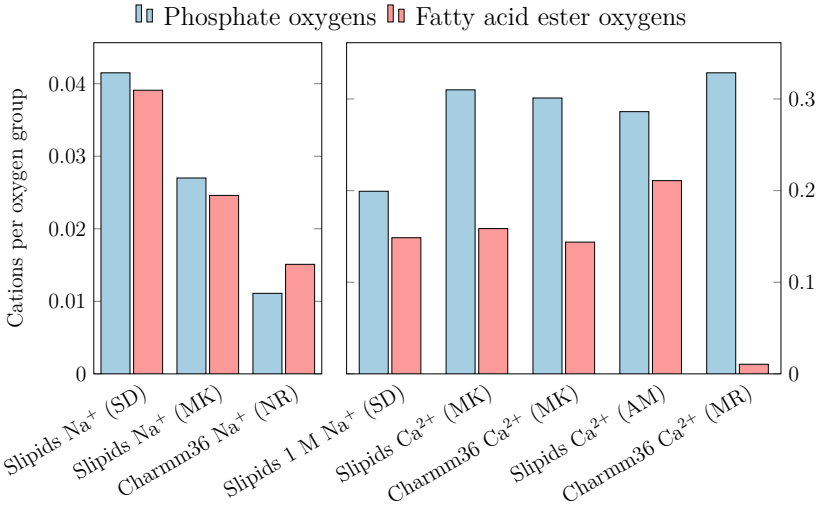

Figure S23: The preferred oxygens with which the ions are in contact. Data for several lipid and ion force fields is shown for the cholesterol-free systems.

S6 Comparison to Earlier Computational Studies

Our results might seem to contradict with recent reports [42, 45] on the effect of cholesterol on the binding of sodium to PC membranes. However, the simulation results in Ref. 42 – when normalized by the number of POPC molecules – provide the same conclusion as our current work, regardless of the authors' claim that cholesterol decreases Na^+ binding. Similarly, we believe that analogous conclusions drawn in Ref. 45 are not substantiated due to the neglect of volume entropy contributions. Namely, the phase space volumes associated with each (discrete) reaction coordinate value are not the same. No attempt to normalize these volumes has been done (which would admittedly be rather difficult), therefore, the direct comparison of free energies between states is not valid. The fact is that only for large cholesterol concentrations (>33%) a slight decrease in sodium binding is observed.

References

[1] Joakim PM Jämbeck and Alexander P Lyubartsev. Another Piece of the Membrane Puzzle: Extending Slipids Further. *Journal of Chemical Theory and Computation*, 9(1):774–784, 2012.

[2] Joakim PM Jämbeck and Alexander P Lyubartsev. Derivation and Systematic Validation of a Refined All-Atom Force Field for Phosphatidylcholine Lipids. *The Journal of Physical Chemistry B*, 116(10): 3164–3179, 2012.

[3] Joakim PM Jämbeck and Alexander P Lyubartsev. An Extension and Further Validation of an All-Atomistic Force Field for Biological Membranes. *Journal of Chemical Theory and Computation*, 8(8): 2938–2948, 2012.

[4] Jeffery B Klauda, Richard M Venable, J Alfredo Freites, Joseph W O'Connor, Douglas J Tobias, Carlos Mondragon-Ramirez, Igor Vorobyov, Alexander D MacKerell Jr, and Richard W Pastor. Update of the CHARMM All-Atom Additive Force Field for Lipids: Validation on Six Lipid Types. *The Journal of Physical Chemistry B*, 114(23):7830–7843, 2010.

[5] Joseph B Lim, Brent Rogaski, and Jeffery B Klauda. Update of the Cholesterol Force Field Parameters in CHARMM. *The Journal of Physical Chemistry B*, 116(1):203–210, 2011.

[6] David E Smith and Liem X Dang. Computer Simulations of NaCl Association in Polarizable Water. *The Journal of Chemical Physics*, 100(5):3757–3766, 1994.

[7] Miriam Kohagen, Philip E Mason, and Pavel Jungwirth. Accurate Description of Calcium Solvation in Concentrated Aqueous Solutions. *The Journal of Physical Chemistry B*, 118(28):7902–7909, 2014.

[8] Sergei Y Noskov and Benoît Roux. Control of Ion Selectivity in LeuT: Two Na^+ Binding Sites With Two Different Mechanisms. *Journal of Molecular Biology*, 377(3):804–818, 2008.

[9] Sylvie Marchand and Benoît Roux. Molecular Dynamics Study of Calbindin D_{9k} in the Apo and Singly and Doubly Calcium-Loaded States. *Proteins: Structure, Function, and Bioinformatics*, 33(2):265–284, 1998.

[10] Sunhwan Jo, Joseph B Lim, Jeffery B Klauda, and Wonpil Im. CHARMM-GUI Membrane Builder for Mixed Bilayers and Its Application to Yeast Membranes. *Biophysical Journal*, 97(1):50–58, 2009.

[11] Jumin Lee, Xi Cheng, Jason M Swails, Min Sun Yeom, Peter K Eastman, Justin A Lemkul, Shuai Wei, Joshua Buckner, Jong Cheol Jeong, Yifei Qi, Sunhwan Jo, Vijay S Pande, David A Case, Charles L Brooks, Alexander D MacKerell Jr, Jeffery B Klauda, and Wonpil Im. CHARMM-GUI Input Generator for NAMD, GROMACS, AMBER, OpenMM, and CHARMM/OpenMM Simulations Using the CHARMM36 Additive Force Field. *Journal of Chemical Theory and Computation*, 12(1):405–413, 2015.

[12] Miriam Kohagen, Philip E Mason, and Pavel Jungwirth. Accounting for Electronic Polarization Effects in Aqueous Sodium Chloride via Molecular Dynamics Aided by Neutron Scattering. *The Journal of Physical Chemistry B*, 2015.

[13] Richard M Venable, Yun Luo, Klaus Gawrisch, Benoît Roux, and Richard W Pastor. Simulations of Anionic Lipid Membranes: Development of Interaction-Specific Ion Parameters and Validation Using NMR Data. *The Journal of Physical Chemistry B*, 117(35):10183–10192, 2013.

[14] Matti Javanainen. POPC with 0, 10, 20, and 30 mol-force field., August 2016. URL `https://doi.org/10.5281/zenodo.60607`.

[15] Matti Javanainen. POPC with 0, 10, 20, and 30 mol-force field., October 2016. URL `https://doi.org/10.5281/zenodo.159759`.

[16] Matti Javanainen. POPC with varying amounts of cholesterol, 130 mM of NaCl. Slipids with ions by Smith & Dang, January 2017. URL `https://doi.org/10.5281/zenodo.259335`.

[17] Matti Javanainen. POPC with varying amounts of cholesterol, 1 M of NaCl. Slipids with ions by Smith & Dang, January 2017. URL `https://doi.org/10.5281/zenodo.259341`.

[18] Matti Javanainen. POPC with varying amounts of cholesterol, 130 mM of NaCl. Slipids with ECC-scaled ions, January 2017. URL `https://doi.org/10.5281/zenodo.259343`.

[19] Matti Javanainen. POPC with varying amounts of cholesterol, 130 mM of NaCl. Charmm36 with default Charmm ions, January 2017. URL `https://doi.org/10.5281/zenodo.259392`.

[20] Matti Javanainen. POPC with varying amounts of cholesterol, 450 mM of CaCl_2. Slipids with ECC-scaled ions, January 2017. URL `https://doi.org/10.5281/zenodo.259354`.

[21] Matti Javanainen. POPC with varying amounts of cholesterol, 450 mM of CaCl_2. Charmm36 with ECC-scaled ions, January 2017. URL `https://doi.org/10.5281/zenodo.259376`.

[22] Matti Javanainen. POPC with varying amounts of cholesterol, 450 mM of CaCl_2. Slipids with default Amber ions, January 2017. URL `https://doi.org/10.5281/zenodo.259349`.

[23] Matti Javanainen. POPC with varying amounts of cholesterol, 450 mM of CaCl_2. Charmm36 with default Charmm ions, January 2017. URL `https://doi.org/10.5281/zenodo.259365`.

[24] Matti Javanainen. Simulations of Na+ and Ca2+ binding to phospholipid membranes, January 2017. URL `https://doi.org/10.5281/zenodo.259443`.

[25] Sarah L Veatch and Sarah L Keller. Separation of Liquid Phases in Giant Vesicles of Ternary Mixtures of Phospholipids and Cholesterol. *Biophysical Journal*, 85(5):3074–3083, 2003.

[26] Giovanni Bussi, Davide Donadio, and Michele Parrinello. Canonical Sampling Through Velocity Rescaling. *The Journal of Chemical Physics*, 126(1):014101, 2007.

[27] Michele Parrinello and Aneesur Rahman. Polymorphic Transitions in Single Crystals: A New Molecular Dynamics Method. *Journal of Applied physics*, 52(12):7182–7190, 1981.

[28] Berk Hess, Henk Bekker, Herman JC Berendsen, and Johannes GEM Fraaije. LINCS: A Linear Constraint Solver for Molecular Simulations. *Journal of Computational Chemistry*, 18(12):1463–1472, 1997.

[29] Tom Darden, Darrin York, and Lee Pedersen. Particle Mesh Ewald: An N·log(N) Method for Ewald Sums in Large Systems. *The Journal of Chemical Physics*, 98(12):10089–10092, 1993.

[30] Ulrich Essmann, Lalith Perera, Max L Berkowitz, Tom Darden, Hsing Lee, and Lee G Pedersen. A Smooth Particle Mesh Ewald Method. *The Journal of Chemical Physics*, 103(19):8577–8593, 1995.

[31] Sander Pronk, Szilárd Páll, Roland Schulz, Per Larsson, Pär Bjelkmar, Rossen Apostolov, Michael R Shirts, Jeremy C Smith, Peter M Kasson, David van der Spoel, Berk Hess, and Erik Lindahl. GROMACS 4.5: A High-Throughput and Highly Parallel Open Source Molecular Simulation Toolkit. *Bioinformatics*, page btt055, 2013.

[32] Shuichi Nosé. A Unified Formulation of the Constant Temperature Molecular Dynamics Methods. *The Journal of Chemical Physics*, 81(1):511–519, 1984.

[33] William G Hoover. Canonical Dynamics: Equilibrium Phase-Space Distributions. *Physical Review A*, 31 (3):1695, 1985.

[34] Mark James Abraham, Teemu Murtola, Roland Schulz, Szilárd Páll, Jeremy C Smith, Berk Hess, and Erik Lindahl. GROMACS: High Performance Molecular Simulations Through Multi-Level Parallelism From Laptops to Supercomputers. *SoftwareX*, 1:19–25, 2015.

[35] Vytautas Gapsys, Bert L de Groot, and Rodolfo Briones. Computational Analysis of Local Membrane Properties. *Journal of Computer-Aided Molecular Design*, 27(10):845–858, 2013.

[36] MATLAB. *version 8.5.0 (R2015a)*. The MathWorks Inc., Natick, Massachusetts, 2015.

[37] T. Parasassi, G. De Stasio, A. d'Ubaldo, and E. Gratton. Phase Fluctuation in Phospholipid Membranes Revealed by Laurdan Fluorescence. *Biophysical Journal*, 57:1179–1186, 1990.

[38] M. L. Horng, J. A. Gardecki, A. Papazyan, and M. Maroncelli. Subpicosecond Measurements of Polar Solvation Dynamics – Coumarin-153 Revisited. *Journal of Physical Chemistry*, 99:17311–17337, 1995.

[39] R. S. Fee and M. Maroncelli. Estimating the Time-Zero Spectrum in Time-Resolved Emission Measurements of Solvation Dynamics. *Chemical Physics*, 183:235–247, 1994.

[40] P. Jurkiewicz, L. Cwiklik, P. Jungwirth, and M. Hof. Lipid Hydration and Mobility: An Interplay Between Fluorescence Solvent Relaxation Experiments and Molecular Dynamics Simulations. *Biochimie*, 94:26–32, 2012.

[41] Hector Martinez-Seara, Tomasz Róg, Marta Pasenkiewicz-Gierula, Ilpo Vattulainen, Mikko Karttunen, and Ramon Reigada. Interplay of Unsaturated Phospholipids and Cholesterol in Membranes: Effect of the Double-Bond Position. *Biophysical Journal*, 95(7):3295–3305, October 2008. ISSN 0006-3495.

[42] Aniket Magarkar, Vivek Dhawan, Paraskevi Kallinteri, Tapani Viitala, Mohammed Elmowafy, Tomasz Róg, and Alex Bunker. Cholesterol Level Affects Surface Charge of Lipid Membranes in Saline Solution. *Scientific Reports*, 4, 2014.

[43] Elzbieta Plesnar, Witold K Subczynski, and Marta Pasenkiewicz-Gierula. Comparative Computer Simulation Study of Cholesterol in Hydrated Unary and Binary Lipid Bilayers and in an Anhydrous Crystal. *The Journal of Physical Chemistry B*, 117(29):8758–8769, 2013.

[44] Christopher C Valley, Jason D Perlmutter, Anthony R Braun, and Jonathan N Sachs. NaCl Interactions With Phosphatidylcholine Bilayers Do Not Alter Membrane Structure but Induce Long-Range Ordering of Ions and Water. *The Journal of Membrane Biology*, 244(1):35–42, 2011.

[45] Jing Yang, Massimiliano Bonomi, Carles Calero, and Jordi Martí. Free Energy Landscapes of Sodium Ions Bound to DMPC-Cholesterol Membrane Surfaces at Infinite Dilution. *Physical Chemistry Chemical Physics*, 18:9036–9041, April 2016. doi: 10.1039/c5cp05527j.